SEMARAK ILMU PUBLISHING

Journal of Advanced Research in Fluid Mechanics and Thermal Sciences

Journal homepage:
https://semarakilmu.com.my/journals/index.php/fluid_mechanics_thermal_sciences/index
ISSN: 2289-7879

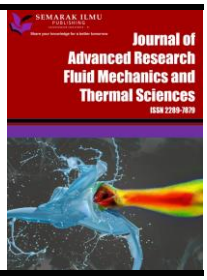

Exploring the Dynamic Behavior of a Tapered Stenosed Artery: An Investigation into Its Unsteady Model

Veena Sreenivasa Beleyur[1,*]

[1] Symbiosis Institute of Technology, Symbiosis International (Deemed University), Lavale – 412 115, Pune, India

ARTICLE INFO

Article history:
Received 16 May 2024
Received in revised form 25 August 2024
Accepted 7 September 2024
Available online 30 September 2024

Keywords:
Blood flow; non-Newtonian; magnetic field; tapered artery; stenosis

ABSTRACT

In this communication, blood flow is considered in a two-phase model of the tapered stenosed artery. Non-Newtonian and Newtonian models are considered in inner and outer regions, respectively. The transverse magnetic field is applied externally on the presumed pulsatile flow of blood to examine the nature of blood flow. It is anticipated that, in the inner region, blood follows the Jeffrey fluid model, and in the outer region, it follows the Bingham Plastic fluid model. The mathematical model of this system is formulated, a non-dimensionalization technique is used, and a numerical solution is obtained using the Finite difference method, one of the most suitable numerical methods for the formulated problem. The expressions for the primary/fundamental characteristics in determining the effect of blood flow are developed to explore the consequence of hematocrit, time component, tapering angle, and magnetic field. Scilab software is employed for mathematical simulations, revealing that flow characteristics within a stenosed artery undergo significant alterations, while the presence of a magnetic field aids in partially regulating the flow characteristics.

1. Introduction

Atherosclerosis, a heart disease, stands as a significant cause of death in the world, including in Western countries. Abnormal and unnatural growth in the artery's inner walls results in the artery's thickening causing stenosed arteries [1-3]. This is the first phase in the development of atherosclerosis, which interrupts blood flow to different parts of the body. Every significant heart disease is because of thick blood. When the blood becomes denser, it can lead to artery damage. In response, the biological system initiates a repair process, during which fatty materials are set down on the artery's inner wall. The primary consequence of arterial stenosis is an increased resistance to blood flow and the associated reduction of blood flow. So, to understand the fundamentals of circulatory disorders, analysis of fluid dynamical characteristics of blood flow is crucial [4].

Although arteries appear to be cylindrical, they are not in reality. They are cylindrical in the beginning, and they may be tapered in the later part as the arteries usually bifurcate. Due to a

* *Corresponding author.*
E-mail address: veena@sitpune.edu.in

https://doi.org/10.37934/arfmts.121.2.4864

decrease in the radius of the artery, there is an increase in pressure, which disrupts the normal blood flow. Therefore, it becomes crucial to investigate blood flow characteristics in a tapered artery [5].

Most studies on blood flow in tapered arteries use the fact that the blood is Newtonian, but in reality, it is not; the flow is primarily non-Newtonian. It acts like Newtonian when it flows through big arteries at a high shear rate, whereas when the radius of the artery is small, in diseased arteries and at a low shear rate, its behavior is always found to be non-Newtonian. In narrow arteries, blood flow is highly pulsatile; the flow is non-Newtonian in the core region, which is a suspension of erythrocytes, and it is Newtonian in the peripheral area, which is the outer region of the artery [6].

Several fluid flow models have been used in blood flow research. The Casson fluid model and Herschel-Bulkley fluid model are two commonly used models of non-Newtonian flow to represent blood flow in the core region of narrow arteries. Herschel-Bulkley model is usually used when the shear rate is low, and this model describes the flow characteristics reasonably well. Also, as this fluid model has additional parameters compared to other non-Newtonian flow models, it is helpful to obtain more thorough facts about the features of blood flow [7]. Jeffrey fluid model is another model which is suitable for non-Newtonian fluids. It has different parameters than other preceding models, which will help get more accurate and realistic results.

Different treatment modalities are available for stenosis-related heart diseases based on various aspects. One of them is the insertion of the catheter, which affects the blood flow and solute dispersion [8]. The other methods include injecting the drug into the blood vessel, which causes the occurrence of a chemical reaction between the drug and blood proteins and affects the effectiveness of the solute transportation in blood flow, applying a magnetic field externally, which regulates the blood flow, etc [9,10]. The existence of hematocrit gives magnetic properties to blood; hence, blood attracts both induced and external magnetic fields, influencing the flow [11,12]. Therefore, the application of magnetic fields is studied in different areas, such as application of external magnetic fields to regulate blood flow, magnetic drug targeting to treat cancer, etc [13,14]. It is recognized in one of the experimentations that the externally applied magnetic field on blood in the direction of flow reduces the viscosity of blood by 20 % – 30 %, and it remains the same almost for more than two hours. Further investigation is required on how and to what level magnets can dilute blood [15]. The thickness of blood is not the same at all times. In non-Newtonian fluid, the thickness fluctuates with the shear rate, inversely or directly, depending on whether the fluid is shear thinning or thickening.

Numerous research scholars have conducted a simulation of blood flow through stenosed tubes. Flow is deliberated as pulsatile during simulation, and diverse models are used to study the flow. Many studies have been conducted comparing 2D and 3D axially symmetric models. The authors discussed how hemodynamic factors play a dynamic role in stenosed arteries. It is witnessed that the magnitude and distribution of wall shear stress are strongly affected by stenosis features, location, and size. It is also seen that resistance to flow and skin friction increases with the highest depth of stenosis, whereas the opposite tendency is observed with increased yield stress. Three-pore model is used to find the role of significant flow characteristics, and it is witnessed that the model can qualitatively capture the plaque change in the intima layer [16-19].

Several numerical procedures, such as the finite volume, finite element, and finite difference methods, are used to investigate the nature of blood flow in a constricted artery by considering blood non–Newtonian. The model is solved by solving Navier–Stoke equations governing the fluid motion. The characteristics of shear-thinning fluid are taken into account to study the nature of blood flow, and it is modeled using different flow models, namely, cross model, generalized power law model, etc. A detailed numerical study is conducted to reach the desired conclusion [20-22].

It is found from the literature that, although the Jeffrey fluid model is used in the studies related to blood flow, in all the studies, it is used for one phase model, and that too mostly in finding the effect of stenosis on blood flow characteristics, but not to regulate the flow in diseased condition using a magnetic field. In the current study, an effort is made to regulate the blood flow in the area affected by stenosis by treating the flow as Jeffrey's fluid model.

This study aims to identify the importance of the transverse magnetic field in regulating the blood flow in tapered stenosed arteries, in which viscosity is one of the leading parameters to be explored. To apply the model in blood rheology, blood viscosity is considered constant in one case and allowed to vary in the other. In the second case, viscosity can vary concerning hematocrit (percentage volume of erythrocytes) to improve the results, which are very close to real-life situations. This study may be helpful for further research, which will help medical practitioners treat the patients of atherosclerosis.

The outline of the paper is as follows. In Section 2, the mathematical problem is formulated in terms of a set of non-linear partial differential equations comprising governing and constitutive equations, viscosity profile, geometry of the model, and initial and boundary conditions. A non-dimensionalization technique is used to simplify the problem thus obtained. Radial transformations are used to streamline the problem further. The model thus obtained is solved using the finite difference method to get the expressions for axial velocity, volumetric flow rate, and wall shear stress in Section 3. Scilab is used for simulation to find the effect of stenosis, tapering angle, magnetic field, time, and hematocrit, and the results are presented in Section 4.

2. Mathematical Formulation

The geometry of the tapered stenosed artery with tapering angle φ is shown in Figure 1. The artery is converging if $\varphi < 0$, diverging if $\varphi > 0$, and the artery is non-tapered if $\varphi = 0$.

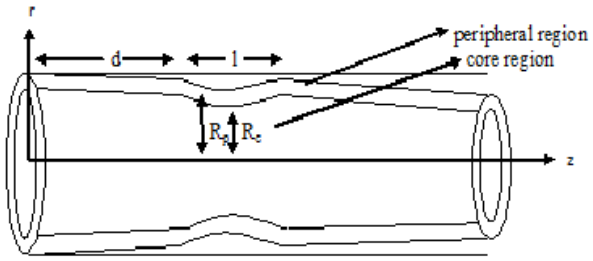

Fig. 1. Schematic representation of tapered two-fluid model

Mathematical system of tapered stenosed arteries in peripheral and core regions are derived respectively as [23]

$$Rp^*(z^*) = \left[\left(md^* + R_p^*\right) + \left\{m - \left(\frac{hp^*}{l^*}\right)\right\}(z^* - d^*) + \left(\frac{hp^*}{(l^*)^2}\right)(z^* - d^*)^2\right] \text{ in } d^* \le z^* \le d^* + l^*$$
$$Rp^*(z^*) = \left(mz^* + R_p^*\right) \text{ in all other cases} \quad (1)$$

$$Rc^*(z^*) = \left[(md^* + R_c^*) + \left\{m - \left(\frac{hc^*}{l^*}\right)\right\}(z^* - d^*) + \left(\frac{hc^*}{(l^*)^2}\right)(z^* - d^*)^2\right] \text{ in } d^* \le z^* \le d^* + l^*$$
$$Rc^*(z^*) = (mz^* + R_c^*) \text{ in all other cases} \quad (2)$$

Here, $Rp^*(z^*)$ and $Rc^*(z^*)$ are radii of the stenosed part of an artery in the peripheral region and core region, respectively, $R_c^* = \gamma R_0^*$ and $R_p^* = R_0^* - R_c^*$ where R_0^*, R_p^*, R_c^* are radii of non-tapered part, peripheral region and core region of the artery. γ is the ratio of radius of the core region to that of the artery, which can vary from 0.95 to 0.98, $m = tan\,\varphi$, hp^* and hc^* are heights of stenosis in peripheral and core region respectively given by $hp^*_{\square} = 4\,\tau_m^*\,sec\,\varphi = 4pR_p^*\sec\varphi$ and $hc^*_{\square} = 4\,\tau_m^*\,sec\,\varphi = 4pR_c^*\sec\varphi$ where p is a real number between 0 and 1, d^* is starting position of stenosis, and l^* is length of stenosis.

It is assumed that blood flow is laminar, unsteady, incompressible, pulsatile, and fully developed. The transverse magnetic field is applied externally, with no induced and negligible electric fields.

The fundamental equation that describes the behavior of the defined system is given by [24]

$$-\frac{\partial P^*}{\partial z^*} + \frac{1}{r^*}\frac{\partial(r^*\tau^*)}{\partial r^*} + kM\frac{\partial H^*}{\partial z^*} = \rho\frac{du^*}{dT^*} \tag{3}$$

Here, u^* is the axial velocity component, r^* is the radial velocity component, τ^* is shear stress, H^* is magnetic field intensity, M is magnetization, k is magnetic permeability, ρ is the density of blood, T^* is time, and p^* is pressure component.

The two-fluid flow model gives more realistic results, the Jeffrey fluid model, a non-Newtonian model, is used in the core region, and the Bingham plastic fluid model is used in the peripheral area. A slight opening stress is given as some initial push is required for the blood to start moving. The corresponding constitutive equations establishing the relationship between key variables in the system are provided by

Jeffrey fluid model [11]:

In the core region, $\tau_c^* = -PI + S$

where τ_c^* is the Cauchy's stress, P is pressure, I is the identity tensor, and S is extra stress.

As *PI* is zero in our problem

$$\tau_c^* = S = \frac{\mu^*}{1+\lambda_1}(\tau^* + \lambda_2\frac{\partial\tau^*}{\partial T^*}) \tag{4}$$

where μ^* is viscosity, λ_2 is retardation time, λ_1 is the ratio of relaxation time to retardation time, and τ^* is shear stress.

Bingham plastic model [25]

In the peripheral region,

$$\tau^* = \tau_0^* + \mu^*\left(-\frac{\partial u^*}{\partial r^*}\right)^{\square} \tag{5}$$

Here τ_0^* is initial stress, μ^* is viscosity of blood.

The viscosity of blood is not constant in the inner region, whereas it is constant in the outer region. It depends on hematocrit, position in the artery, and the stage of disease [26]. Einstein's

formula, which defines the viscosity profile applicable for the dilute suspension of spherical shape erythrocytes, is

$$\mu^* = \mu_0^* [\, 1 + \beta \times He \left(1 - \left(\frac{r^*}{R_0^*}\right)^q \right)] \tag{6}$$

Here, $q \geq 2$ is the parameter that governs the shape of the viscosity profile for blood. He is the hematocrit, which is different for different people, usually ranges from 25% to $50\ \%$, μ_0^*= viscosity of plasma, β is a constant equal to 2.5 for blood.

The boundary conditions considered for the study as

$$u^* = 0\ at\ r^* = R_p^*(z^*) \text{ and } \frac{\partial u^*}{\partial r^*} = 0\ at\ r^* = 0 \tag{7}$$

$$u_c^* = u_p^*\ at\ r^* = R_c^*(z^*)\ and\ \tau_{core}^* = \tau_{peri}^*\ at\ r^* = R_c^* \tag{8}$$

The initial conditions are $u_c^* = u_p^* = 0\ at\ T^* = 0$ (9)

The equation for pulsatile flow is captured as [27],

$$-\frac{\partial p^*}{\partial z^*} = A_0^* + A_1^* \cos w^* T^* \tag{10}$$

Here, $w^* = 2\pi f_p^*$, f_p^* is pulsatile frequency, $and\ A_0^*$ and A_1^* are constant and pulsatile pressure gradient amplitudes, respectively.

3. Solution Procedure

A dimensionless system is a mathematical technique that reduces the number of variables and parameters, which helps understand the underlying physics or relationships among variables. Below is the system used in this problem.

$$r^* = rR_0 \quad z^* = zR_0 \quad R^* = RR_0 \quad T = T^* w^* \quad d^* = dR_0 \quad l^* = lR_0 \quad P^* = P\rho u_0^2$$
$$u^* = uu_0 \quad \tau^* = \tau\rho u_0^2 \quad \tau_c^* = \tau_c \rho u_0^2 \quad H^* = HH_0 \quad h^* = hR_0 \quad \mu^* = \mu\rho u_0 R_0 \quad R_p^* = R_p R_0$$
$$\mu_0^* = \mu_0 \rho u_0 R_0 \quad A^* = \frac{\rho u_0^2}{R_0} A \quad w^* = wt_0 \tag{11}$$

Applying (11) in (1) to (10), we get

The geometry of the stenosed artery in the outer and inner region (respectively) becomes.

$$R_p(z) = \left\{ (R_0 + md) + \left[m - \left(\frac{hp}{l}\right) \right] (z - d) + \left(\frac{hp}{l^2}\right) (z - d)^2 \right\} \text{ in } d \leq z \leq d + l$$
$$R_p(z) = R_0 + mz \quad \text{otherwise} \tag{12}$$

$$R_c(z) = \left\{ (R_c + md) + \left[m - \left(\frac{hc}{l}\right) \right] (z - d) + \left(\frac{hc}{l^2}\right) (z - d)^2 \right\} \text{ in } d \leq z \leq d + l$$
$$R_c(z) = R_c + mz \quad \text{otherwise} \tag{13}$$

Here, $hp = 4p\,R_p \sec\varphi,\ hc = 4p\,\mathrm{R_c}\sec\ \varphi\,, R_c = \gamma R_0$ and $R_p = R_0 - R_c, p$ is a real number that helps to determine the severity of stenosis, which lies in (0, 1).

The governing equation becomes

$$-\frac{\partial P}{\partial z} + \frac{1}{r}\frac{\partial(r\tau)}{\partial r} + \frac{KMH_0}{\rho u_0^2}\frac{dH}{dZ} = \frac{wR_0}{u_0}\frac{du}{dT} \tag{14}$$

The constitutive equations in the inner and outer regions are, respectively,

Jeffrey fluid model

Extra stress S is defined as

$$\tau_c^{\square} = S = \frac{\mu\rho u_0 R_0}{1+\lambda_1}(\tau + \lambda_2 wt_0\frac{\partial\tau}{\partial T}) \tag{15}$$

where μ is viscosity, λ_2 is retardation time, λ_1 is the ratio of relaxation time to retardation time, and τ is shear stress.

Bingham plastic model: $\tau = \tau_0 + \mu^{\square}\left(-\frac{\partial u}{\partial r}\right)^{\square}$ (16)

Then Eq. (6) becomes $\mu = \mu_0[\,1 + \beta \times He\,\left(\,1 - \left(\frac{r}{\mathrm{R_0}}\right)^q\right)]$ (17)

In the Bingham plastic model (in the peripheral region), $\frac{r}{\mathrm{R_0}}$ tends to 1; hence, $\left(\frac{r}{\mathrm{R_0}}\right)^q$ tends to 1.

So, $\mu = \mu_0$ implies $\tau = \tau_0 + \mu_0{}^{\square}\left(-\frac{\partial u}{\partial r}\right)^{\square}$ (18)

The boundary conditions are

$u = 0$ at $r = R_p(z)$ and $\frac{\partial u}{\partial r} = 0$ at $r\ =\ 0$ (19)

$u_c = u_p\ at\ r = R_c(z)\ and\ \tau_{core} = \tau_{peri}\ at\ r = R_c(z)$ (20)

The initial conditions are $u_c = u_p = 0$ at $T = 0$ (21)

The equation for pulsatile flow is $-\frac{\partial p^{\square}}{\partial z^{\square}} = A_0 + A_1\cos T$ (22)

Radial transformation given by, $x = \frac{r}{R_0}\ ,\ t = \frac{T}{t_0}$ (23)

The governing equation becomes, $-\frac{\partial P}{\partial Z} + \frac{1}{xR_0}\frac{\partial(x\tau)}{\partial x} + \frac{KMH_0}{\rho u_0^2}\frac{dH}{dZ} = \frac{wR_0}{u_0}\frac{\partial u}{\partial t}$ (24)

The constitutive equations become

Jeffrey fluid

$$\tau_c^{\square} = S = \frac{\mu\rho u_0 R_0}{1+\lambda_1}(\tau + \lambda_2 t_0 \frac{\partial \tau}{\partial t}) \tag{25}$$

Bingham plastic model

$$\tau = \tau_0 + \frac{\mu_0}{R_0}\left(-\frac{\partial u}{\partial x}\right)^{\square} \tag{26}$$

The Einstein's equation becomes

$$\mu = \mu_0[\,1 + \beta \times He\,(\,1 - (x)^q)] \tag{27}$$

Boundary conditions becomes

$$u = 0 \text{ at } x = \frac{R_p(z)}{R_0} \text{ and } \frac{\partial u}{\partial x} = 0 \text{ at } x = 0 \tag{28}$$

$$u_c = u_p \text{ at } x = \frac{R_c(z)}{R_0} \text{ and } \tau_{core} = \tau_{peri} \text{ at } x = \frac{R_c(z)}{R_0} \tag{29}$$

Initial conditions becomes

$$u_c = u_p = 0 \text{ at } t = 0 \tag{30}$$

The pulsatile flow equation becomes

$$-\frac{\partial p^{\square}}{\partial z^{\square}} = A_0 + A_1 \cos t t_0 \tag{31}$$

Using (25) and (27) in (24), we get

$$\begin{aligned}&\frac{\tau_0\rho u_0\mu_0}{x(1+\lambda_1)}[(1+\beta.He)-(q+1)x^q] - \frac{\tau_0\rho u_0\mu_0^2}{x(1+\lambda_1)R_0}[(1+\beta.He)-(q+1)x^q]\left(-\frac{\partial^2 u}{\partial x^2}\right)\\ &-\frac{\rho u_0\mu_0 R_0}{(1+\lambda_1)}[(1+\beta.He)-(q+1)x^q]\left(\frac{\partial u}{\partial x}\right)+\frac{\lambda_2 t_0\mu_0}{xR_0^2}\left(-\frac{\partial^2 u}{\partial x^2}\right)\left(\frac{\partial u}{\partial t}\right)\\ &-\frac{\partial P}{\partial Z}+\frac{kMH_0}{\rho u_0^2}\frac{dH}{dz} = \frac{wR_0}{u_0}\frac{\partial u}{\partial t}\end{aligned} \tag{32}$$

Using (26) and (31) in (24)

$$\frac{1}{xR_0}\left[\tau_0 + \left(\frac{\mu_0}{R_0}\right)^{\square}\left(-\frac{\partial^2 u}{\partial x^2}\right)\right] + \frac{kMH_0}{\rho u_0^2}\frac{dH}{dz} - \frac{\partial P}{\partial Z} = \frac{wR_0}{u_0}\frac{\partial u}{\partial t} \tag{33}$$

Eq. (32) gives axial velocity in the core region, and (33) shows the same in the peripheral area. There are quite a few numerical approaches for solving a system of non-linear partial differential equations. One of the most widely used methods is the Finite difference method. This method

discretizes the Eq. (32) and Eq. (33). $u(x,z,t)$ is discretized into $u(x_i,z_j,t_k)$ and denoted by $u_{i,j}^k$. The increment in the radial direction is denoted as Δx, the increment in the axial direction as Δz, and the increment in the time component as Δt. The central difference scheme is used for spatial derivatives, and the forward difference scheme is used for time derivatives.

$$\frac{\partial u_m}{\partial x} = \frac{(u_m)_{i,j+1}^k - (u_m)_{i,j-1}^k}{2\,\Delta x} \tag{34}$$

$$\frac{\partial^2 u_m}{\partial x^2} = \frac{(u_m)_{i,j+1}^k + (u_m)_{i,j-1}^k - 2(u_m)_{i,j}^k}{(\Delta x)^2} \tag{35}$$

$$\frac{\partial u_m}{\partial t} = \frac{(u_m)_{i,j}^{k+1} - (u_m)_{i,j-1}^k}{\Delta t} \tag{36}$$

Here, $m = C$ if $0 < x < \alpha$ and $m = N$ if $\alpha < x < 1$, we define $x_j = (j-1)\,\Delta x$ for $j = 1, 2, \ldots, C, C+1$ such that $x_{C+1} = \alpha$ and $x_j = \alpha + [j - (C+1)]\,\Delta x$ for $j = C+1, C+2, \ldots, N+1$ such that $x_{N+1} = 1$, $z_i = (i-1)\,\Delta z$ for $i = 1, 2, \ldots$ and $t_k = (k-1)\,\Delta t, k = 1, 2, \ldots$

Using (34), (35), and (36) in (32), we get

$$\begin{aligned}(u_c)_{i,j}^{k+1} = {} & (u_c)_{i,j}^k + \Delta t\left[-\frac{u_0}{wR_0}\left(\frac{\partial p}{\partial z}\right)_i^k + \frac{u_0}{wR_0}\frac{kMH_0}{\rho u_0^2}\frac{dH}{dz}\right] \\ & + \Delta t\left[\frac{u_0}{wR_0}\frac{\tau_0\rho u_0\mu_0}{x_i(1+\lambda_1)}[(1+\beta.He) - (q+1)(x_i)^q]\right] \\ & + \Delta t\left[\frac{u_0}{wR_0}\frac{\tau_0\rho u_0\mu_0^2}{x_i(1+\lambda_1)R_0}[(1+\beta.He) \right. \\ & \left. - (q+1)(x_i)^q]\right]\left[\frac{(u_c)_{i,j+1}^k + (u_c)_{i,j-1}^k - 2(u_c)_{i,j}^k}{(\Delta x)^2}\right] \\ & + \Delta t\left[\frac{u_0}{wR_0}\frac{\rho u_0\mu_0 R_0}{(1+\lambda_1)}[(1+\beta.He) - (q+1)(x_i)^q]\right]\left[\frac{(u_c)_{i,j+1}^k - (u_c)_{i,j-1}^k}{2\,\Delta x}\right] \\ & - \Delta t\left[\frac{u_0}{wR_0}\frac{\lambda_2 t_0\mu_0}{x_i R_0^2}\right]\left[\frac{(u_c)_{i,j+1}^k + (u_c)_{i,j-1}^k - 2(u_c)_{i,j}^k}{(\Delta x)^2}\right]\left[\frac{(u_c)_{i,j}^{k+1} - (u_c)_{i,j-1}^k}{\Delta t}\right]\end{aligned} \tag{37}$$

Using (34), (35), and (36) in (33), we get,

$$\begin{aligned}(u_p)_{i,j}^{k+1} = {} & (u_p)_{i,j}^k + \Delta t\left(\frac{u_0}{wR_0}\frac{kMH_0}{\rho u_0^2}\frac{dH}{dz}\right) + \Delta t\left(\frac{u_0}{wR_0}\right)\left(\frac{\partial p}{\partial z}\right)_i^k \\ & + \Delta t\left(\frac{u_0}{wR_0}\frac{1}{x_i R_0}\left[\tau_{0-}\left(\frac{\mu_0}{R_0}\right)\left(\frac{(u_p)_{i+1,j}^k + (u_p)_{i-1,j}^k - 2(u_p)_{i,j}^k}{(\Delta x)^2}\right)^{\square}\right]\right)\end{aligned} \tag{38}$$

Similarly, we get the expressions for volumetric flow rate and wall shear stress as,

$$Q_i^k = 2\pi\left[\int_0^\alpha x_j (u_c)_{i,j}^{k\,\square}\, dx_j + \int_\alpha^1 x_j (u_p)_{i,j}^{k\,\square}\, dx_j\right] \tag{39}$$

$$\tau_i^k = \tau_0 - \mu\left(\frac{(u_p)_{i,j+1}^k - (u_p)_{i,j-1}^k}{2\,\Delta x}\right) \tag{40}$$

4. Result and Discussion

This study aims to notice the impact of tapering angle, non-Newtonian nature, yield stress, magnetic field, and pulsatile nature on the most critical blood flow characteristics through the tapered stenosed artery. The subsequent values as shown in Table 1 are used for computations.

Table 1
Values of the parameters

Parameter	Value	Parameter	Value
n	0.95 and 1.05	$\frac{dH}{dZ}$	0, 10000, 20000, 30000
τ_0	0.02	u_0	36 cm/sec
d	2 cm	A_0	100 kg/m^{-2} s^{-2}
l	5 cm	A_1	0.2 A_0
ρ	1.06 gm / cm^3	f_p	1.2 Hz
R_0	0.25 cm	Δx	0.0125
k	1	Δz	0.1
M	2 amp/sec	Δt	0.0125
t_0	100	μ	3.5 cP
μ_0	1.8 cP	β	2.5
He	20 % to 50 %	q	2
φ	±0.01, ±0.015	γ	0.95 to 0.98
t	0.1, 02,…,0.85 sec	H_0	0.2 Tesla

4.1 Axial Velocity

Axial velocity is an essential factor that needs to be regulated to avoid further complications in diseased arteries. There is a requirement to balance a lot of parameters to regulate velocity. The movement of blood flow in the core region in both diverging and converging arteries is shown in Figure 2 for different magnetic field gradients. It is noted that axial velocity reduces as r increases for smaller gradients. Axial velocity at $r = 0.2$ in the diverging artery and at $r = 0.12$ in the converging artery are the same irrespective of the gradient of the magnetic field. Axial velocity stabilizes for higher values of gradients ($H = 40000$).

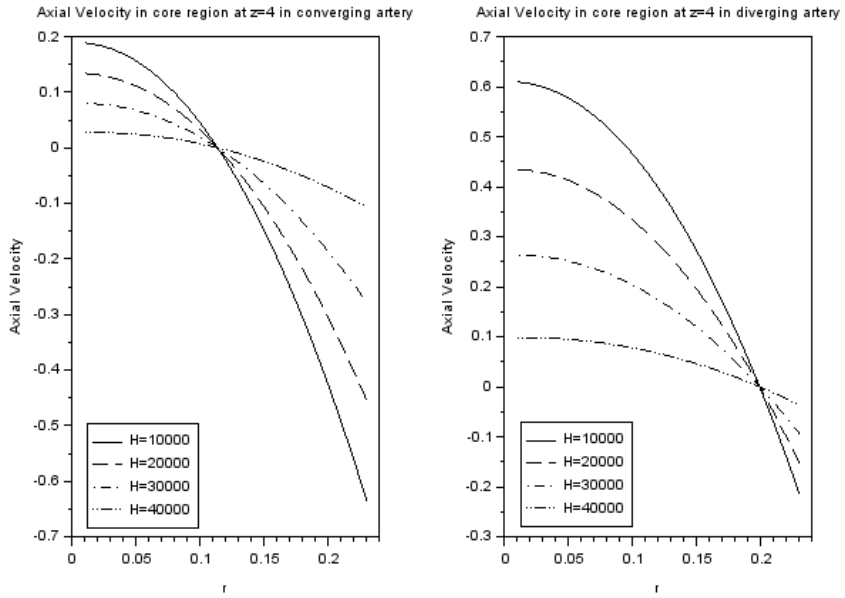

Fig. 2. Axial velocity in the inner region for different gradients

Figure 3 illustrates the trend of axial velocity in the core region for different r. Axial velocity decreases steadily as z increases from 3 to 5, then increases in the converging artery. In contrast, a slight decrease is observed in the beginning and a drastic increase later in the case of the diverging artery.

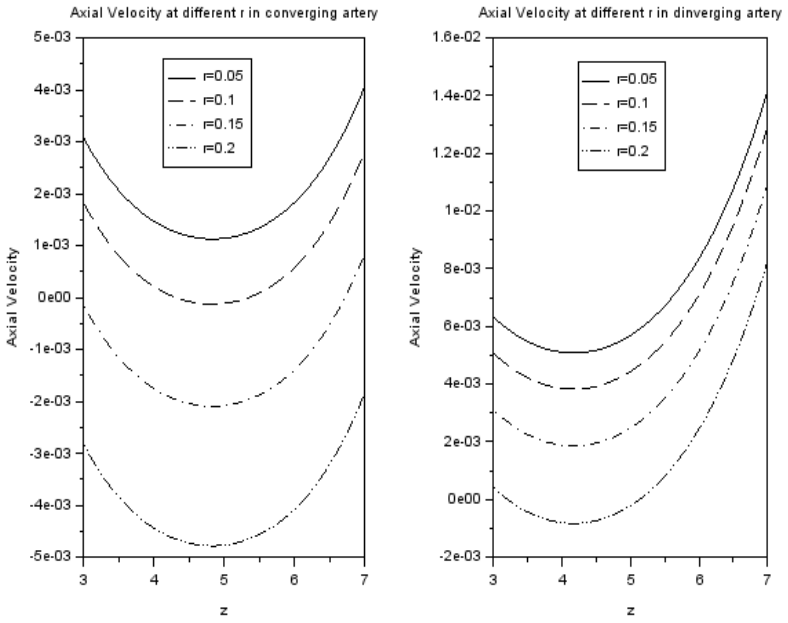

Fig. 3. Axial velocity in the core region for different r

It is established from Figure 4 that the axial velocity is linear and inversely proportional to r. Lower axial velocity is observed with increasing gradient in the diverging artery, and a precisely opposite trend is observed in the converging artery.

In all these cases, the velocity is higher for higher values of Jeffrey parameter λ_1. Velocity is less when λ_1 is small (between 0 and 1). As λ_1 increases further from 1 to 2, velocity rises significantly. The velocity drops down to zero at the throat of the stenosis; the rate of decrease is higher in the latter case.

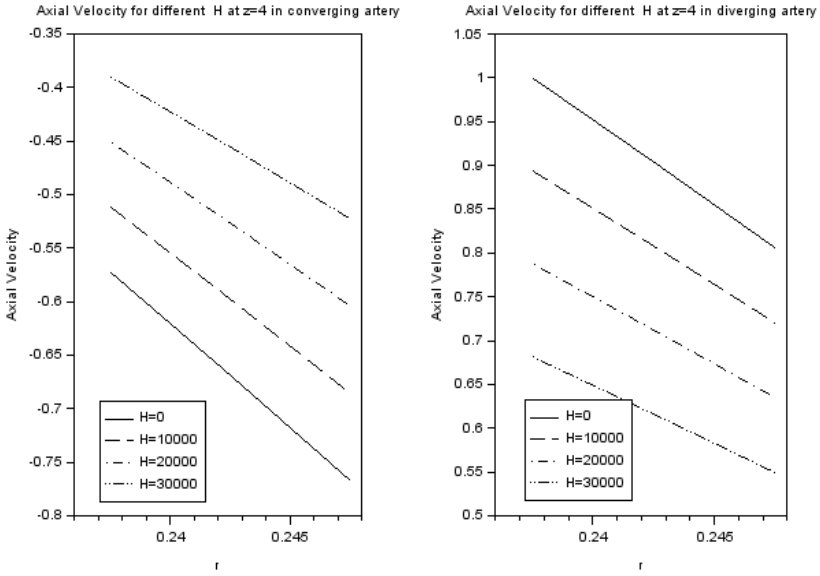

Fig. 4. Axial velocity in the outer region for different gradients

Figure 5 displays the behavior of velocity against viscosity at $z = 2.5$ in converging and diverging arteries. Radial coordinate and hematocrit are two factors that influence the viscosity. Axial velocity is inversely proportional to viscosity. Viscosity is low near the radial line of the artery. Hence, there is a negligible difference in velocity, and as we move away from the radial line, the rate of change of velocity is higher.

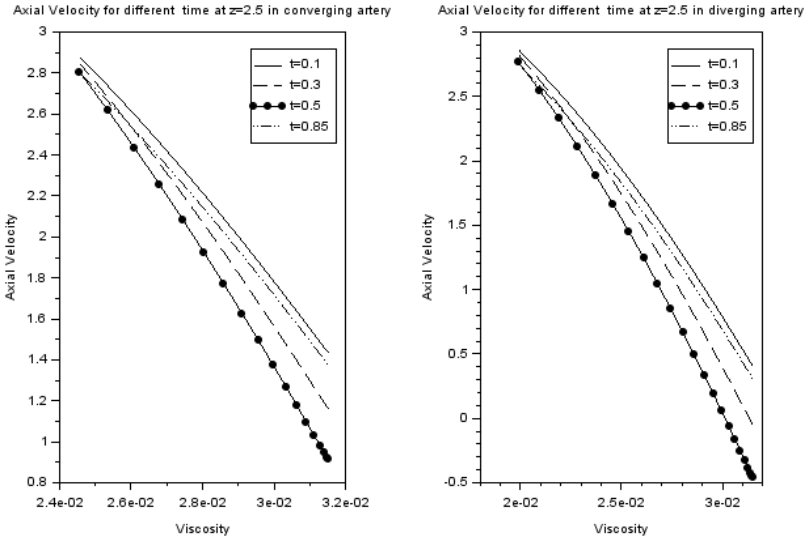

Fig. 5. Axial velocity in the inner region at $z = 2.5$

Figure 6 represents a comparative velocity profile at $z = 4$ in the core region. Velocity drops as we move from the radial line to the stenosis wall and becomes zero at the end. It is required to manage Jeffrey parameters to raise / lower / balance velocity along with other vital parameters related to magnetization.

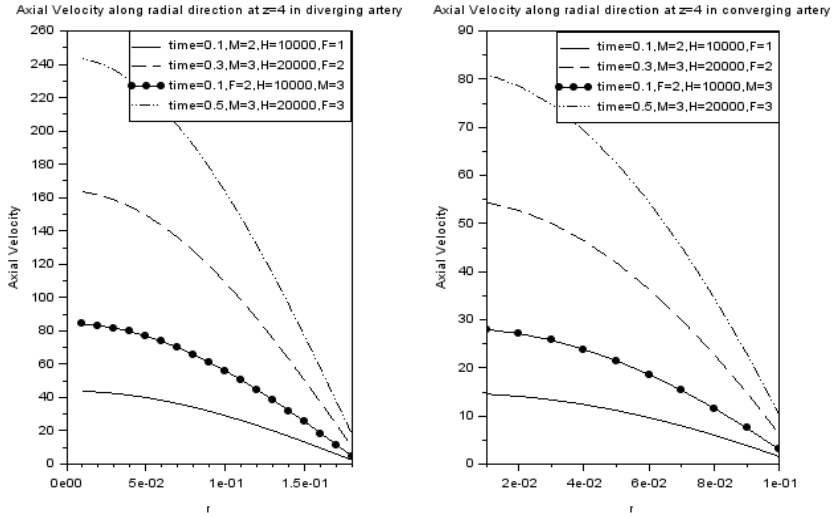

Fig. 6. Axial velocity in the core region at $z = 4$

The percentage of hematocrit is varied to observe the velocity behavior. A significant variation in velocity is observed in diverging arteries for different hematocrit values, which is not the case in converging arteries (Figure 7). A higher hematocrit level helps to increase the velocity near the center line of the artery.

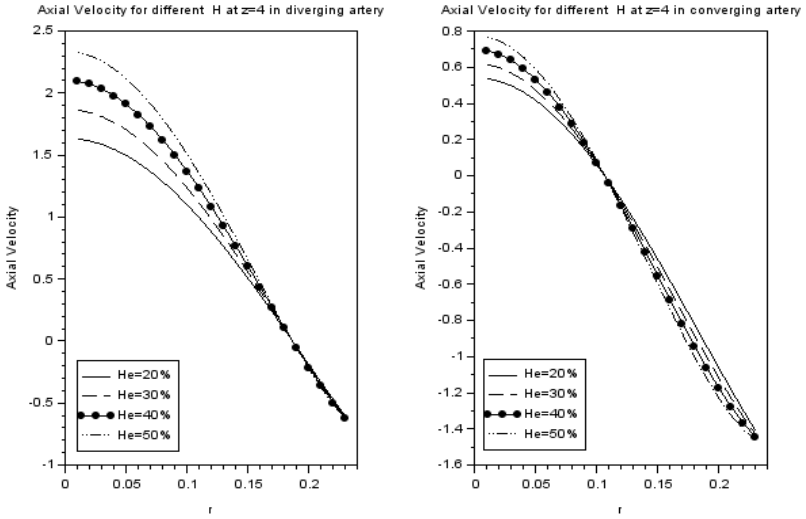

Fig. 7. Axial velocity in the core region for different hematocrit at $z = 4$

4.2 Volumetric Flow Rate

Figure 8 elucidates the rate of change in flow rate for the fixed tapering angle in diverging and converging arteries. Initially, the flow rate decreases quickly in the converging artery compared to the diverging artery. In the next phase, the increase in flow rate is low in the narrowing arteries and high in the widening arteries.

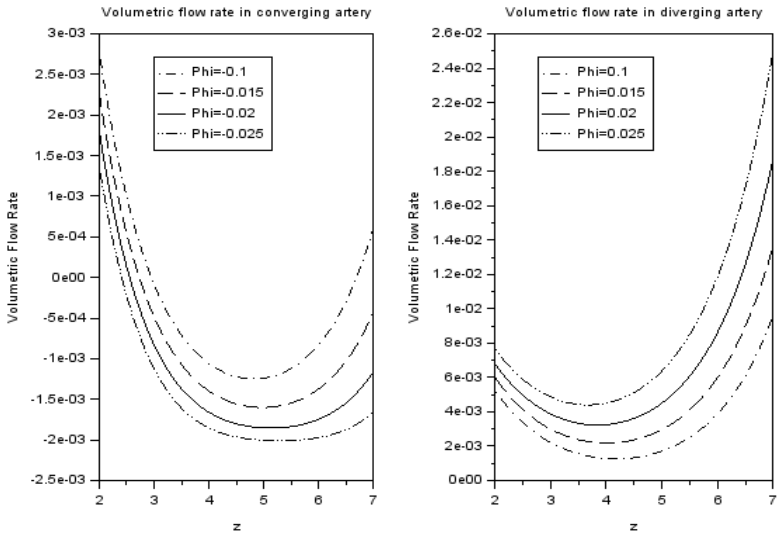

Fig. 8. Flow rate for different tapering angle

Figure 9 represents the style of flow rate with respect to time factor. The increase in flow rate with respect to t is more significant at the ends of stenosis in the diverging artery. In contrast, in the converging artery, even though the flow rate increases as t increases at the ends, it decreases in the middle of stenosis. Significant variation is observed at the throat in the converging artery, and no change in the diverging artery as the artery is widened.

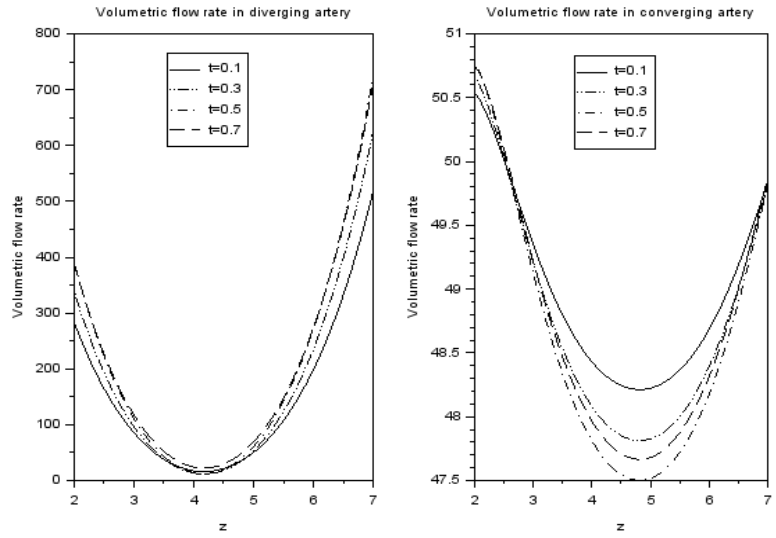

Fig. 9. Flow rate for different time

A comparative visualization is given in Figure 10. The result in the diverging artery indicates that the stenosis, or narrowing, has a relatively small impact on the volumetric flow rate. A significant change is observed in the converging artery to contradict this story. This means that tapering angle, time, and magnetization parameters strongly influence the volumetric flow rate in narrowing arteries. The results suggest optimizing and controlling these factors is essential to ensure a stable and desired flow rate in narrowing arteries.

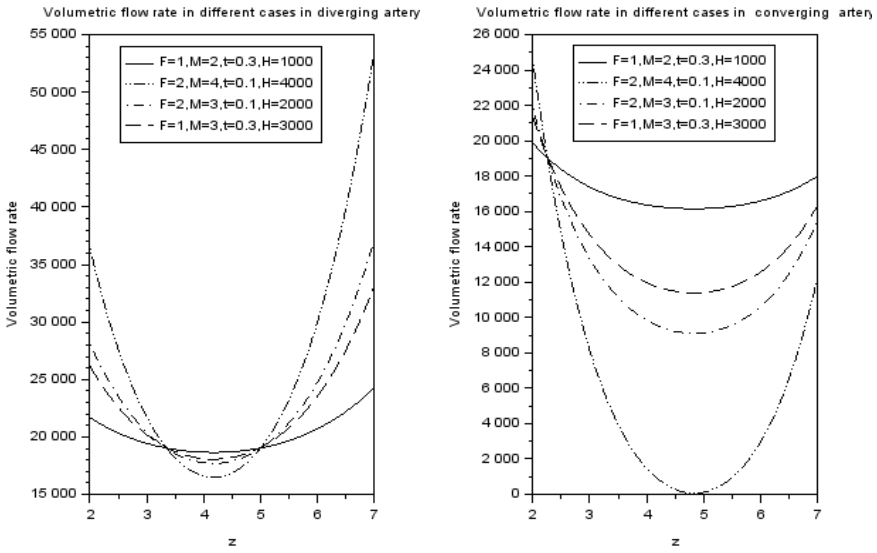

Fig. 10. Volumetric flow rate in different cases

Figure 11 demonstrates the flow rate trend for different gradients by varying viscosity. The viscosity is assumed to vary w.r.t. position, i.e., radial coordinate. The flow rate decreases in the first half and then increases after the stenosis peak. A turn in the profile is observed in the diverging artery between $z = 3$ and $z = 5$. There is no notable change as viscosity varies w.r.t. hematocrit, which is not displayed in the figure.

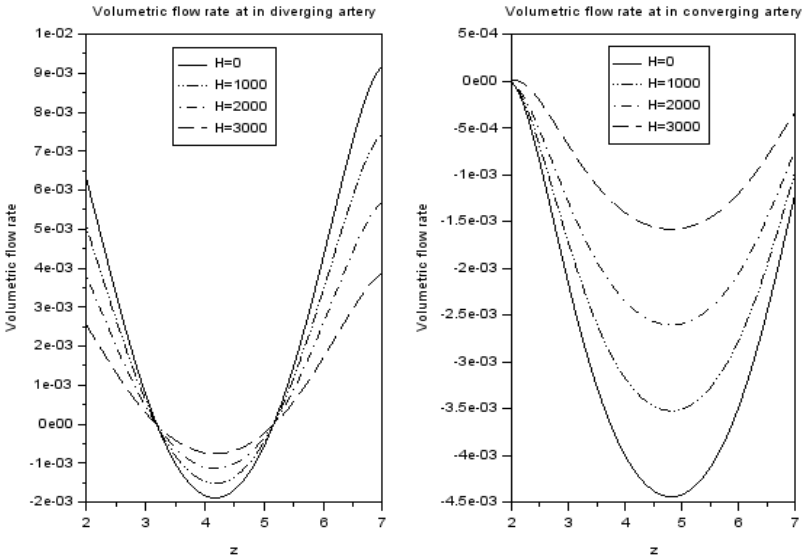

Fig. 11. Flow rate for different gradients

4.3 Wall Shear Stress

The time (t) parameter is considered while drawing Figure 12. Accordingly, it is observed that shear stress decreases as t increases from 0.1 to 0.5. The stress starts increasing from t=0.7 again. In addition to this, it is noticed that shear stress is higher in converging arteries than in diverging arteries.

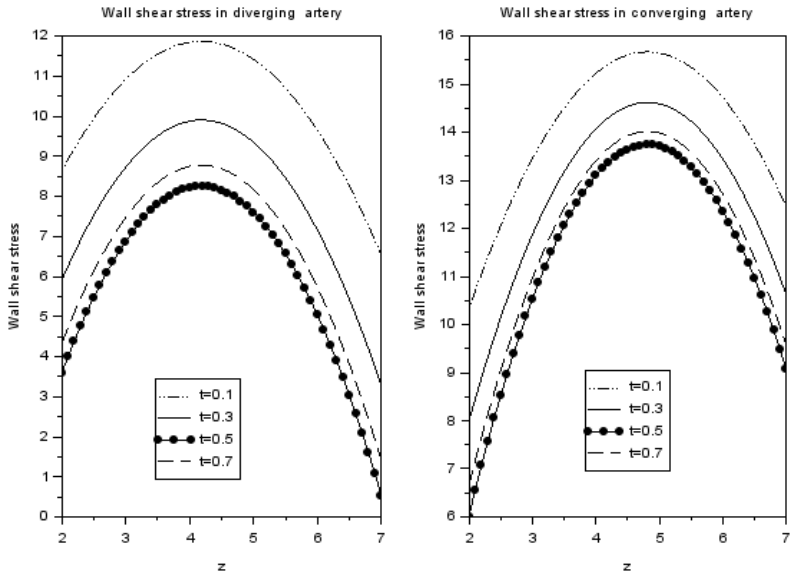

Fig. 12. Shear stress for different t

The wall shear stress is analyzed for two values of magnetic field gradient, 10000 and 20000, and the results can be observed in Figure 13. Magnetization, tapering angle, and time play a crucial role in shaping the profile of wall shear stress. There is no significant difference, although there is a difference in gradient values. In other words, we can conclude the influence of magnetic field gradient is insignificant on shear stress.

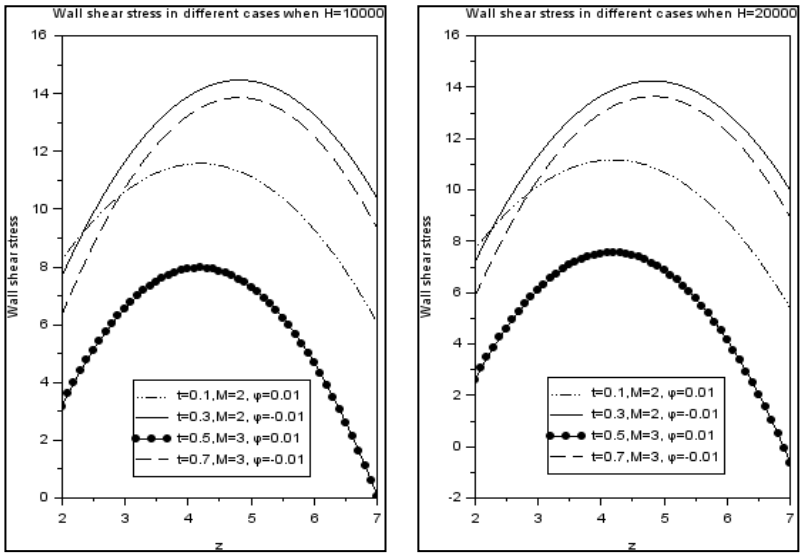

Fig. 13. Shear stress for $\frac{dH}{dZ}(H) = 10000$ and $\frac{dH}{dZ}(H) = 20000$

5. Conclusion

This study discusses the effect of a magnetic field on the flow characteristics of blood flow through tapered stenosed arteries. The flow is deemed to be unsteady and two-dimensional. The study focuses on estimating the connection between arterial disease and biomechanics by examining the influence of magnetization, tapering angle, relaxation, and retardation time.

The study results show that the vital characteristics of blood flow through stenosed arteries are affected. The results obtained agree with previous findings, indicating the validity of the approach.

The study reveals that the externally applied magnetic field strongly influences flow rate and axial velocity. Conversely, its significance is much lower in the case of shear stress. In other words, the magnetic field significantly impacts blood's movement and flow rate. Still, its effect on the force experienced by the artery walls is relatively tiny.

The results found in this study can predict the behavior of significant characteristics of blood flow in different conditions. These parameters support stabilizing the flow and are visualized in the figures. These points make the study valuable for medical practitioners as they can use this information to develop new treatment approaches for atherosclerosis, a condition characterized by the narrowing of arteries due to plaque buildup. By understanding how blood flow is affected in stenosed arteries and the influence of factors such as magnetization, tapering angle, and time, medical practitioners can develop more effective treatment modalities for associated ailments.

Furthermore, there are several characteristics of blood flow and numerous parameters affecting the flow of blood in stenosed arteries, and the current study examined three crucial characteristics, axial velocity, flow rate, and wall shear stress, by varying a few parameters. There is a scope to study the remaining characteristics of blood flow by varying other parameters so that the result will be more specific and it is possible to get a clear idea of how much magnetic field is required to regulate the blood flow in the stenosed artery.

References

[1] Bali, Rekha, and Usha Awasthi. "Mathematical model of blood flow in small blood vessel in the presence of magnetic field." *Applied Mathematics* 2, no. 02 (2011): 264-269. https://doi.org/10.4236/am.2011.22031

[2] Sankar, D. S., and Yazariah Yatim. "Comparative analysis of mathematical models for blood flow in tapered constricted arteries." In *Abstract and Applied Analysis*, vol. 2012, no. 1, p. 235960. Hindawi Publishing Corporation, 2012. https://doi.org/10.1155/2012/235960

[3] Sankar, D. S., and Usik Lee. "FDM analysis for MHD flow of a non-Newtonian fluid for blood flow in stenosed arteries." *Journal of Mechanical Science and Technology* 25 (2011): 2573-2581. https://doi.org/10.1007/s12206-011-0728-x

[4] Tu, Cheng, and Michel Deville. "Pulsatile flow of non-Newtonian fluids through arterial stenoses." *Journal of Biomechanics* 29, no. 7 (1996): 899-908. https://doi.org/10.1016/0021-9290(95)00151-4

[5] Dwivedi, A. P., T. S. Pal, and L. Rakesh. "Micropolar fluid model for blood flow through a small tapered tube." *Indian Journal of Technology* 20, no. 8 (1982): 295-299.

[6] Siddiqui, S. U., N. K. Verma, Shailesh Mishra, and R. S. Gupta. "Mathematical modelling of pulsatile flow of Casson's fluid in arterial stenosis." *Applied Mathematics and Computation* 210, no. 1 (2009): 1-10. https://doi.org/10.1016/j.amc.2007.05.070

[7] Chhabra, Rajendra P. "Non-Newtonian fluids: an introduction." *Rheology of Complex Fluids* (2010): 3-34. https://doi.org/10.1007/978-1-4419-6494-6_1

[8] Munir, Intan Diyana, Nurul Aini Jaafar, and Sharidan Shafie. "Effect of Catheter and Stenosis on Solute Diffusion in Non-Newtonian Blood Flow through a Catheterized Stenosed Artery." *CFD Letters* 14, no. 12 (2022): 11-26. https://doi.org/10.37934/cfdl.14.12.1126

[9] Jaafar, Nurul Aini, Siti NurulAifa Mohd ZainulAbidin, Zuhaila Ismail, and Ahmad Qushairi Mohamad. "Mathematical analysis of unsteady solute dispersion with chemical reaction through a stenosed artery." *Journal of Advanced Research in Fluid Mechanics and Thermal Sciences* 86, no. 2 (2021): 56-73. https://doi.org/10.37934/arfmts.86.2.5673

[10] Lahonian, Mansour, Sepideh Khedri, Saman Aminian, Leyla Ranjbari, and Aram Ardalan. "Effect of Particle-Particle and RBC-Particle Interactions on Capture Efficiency of Magnetic Nanocarriers Under the Influence of a Nonuniform Magnetic Field." *Iranian Journal of Science and Technology, Transactions of Mechanical Engineering* 48, no. 2 (2024): 461-474. https://doi.org/10.1007/s40997-023-00669-3

[11] Nallapu, Santhosh, and G. Radhakrishnamacharya. "Flow of Jeffrey Fluid through Narrow Tubes." *arXiv preprint arXiv:1403.7695* (2014). https://doi.org/10.1155/2014/713831

[12] Veena, B. S., and Arundhati S. Warke. "Study of blood flow in one half of cosine shaped stenosis in the presence of magnetic field." *International Journal of Experimental and Computational Biomechanics* 3, no. 2 (2015): 121-136. https://doi.org/10.1504/IJECB.2015.070435

[13] Alizadeh, As' ad, Saman Aminian, Asal Malakshahi, Aram Ardalan, Mansour Lahonian, Mohammad Najafi, and Kavan Zarei. "Numerical investigation of the injection angle of carrier nanoparticles under the effect of different magnetic fields." *Journal of Magnetism and Magnetic Materials* 578 (2023): 170836. https://doi.org/10.1016/j.jmmm.2023.170836

[14] Aram, Ardalan, Aminan Saman, and Lahonian Mansour. "The Effect of the Non-Newtonian Behavior of Blood on Capture Efficiency of Particles in a Vessel with a Local Symmetrical Stenosis." *BioNanoScience* (2024): 1-11. https://doi.org/10.1007/s12668-024-01304-4

[15] Tao, R., and Ke Huang. "Reducing blood viscosity with magnetic fields." *Physical Review E-Statistical, Nonlinear, and Soft Matter Physics* 84, no. 1 (2011): 011905. https://doi.org/10.1103/PhysRevE.84.011905

[16] Karimi, Safoora, Mitra Dadvar, Mahsa Dabagh, Payman Jalali, Hamid Modarress, and Bahram Dabir. "Simulation of pulsatile blood flow through stenotic artery considering different blood rheologies: comparison of 3d and 2d-axisymmetric models." *Biomedical Engineering: Applications, Basis and Communications* 25, no. 02 (2013): 1350023. https://doi.org/10.4015/S1016237213500233

[17] Dabagh, Mahsa, Paritosh Vasava, and Payman Jalali. "Effects of severity and location of stenosis on the hemodynamics in human aorta and its branches." *Medical & Biological Engineering & Computing* 53 (2015): 463-476. https://doi.org/10.1007/s11517-015-1253-3

[18] Venkatesan, Jayavelu, D. S. Sankar, K. Hemalatha, and Yazariah Yatim. "Mathematical analysis of Casson fluid model for blood rheology in stenosed narrow arteries." *Journal of Applied Mathematics* 2013, no. 1 (2013): 583809. https://doi.org/10.1155/2013/583809

[19] Cilla, Myriam, Estefania Pena, and Miguel A. Martinez. "Mathematical modelling of atheroma plaque formation and development in coronary arteries." *Journal of The Royal Society Interface* 11, no. 90 (2014): 20130866. https://doi.org/10.1098/rsif.2013.0866

[20] Achaba, Louiza, Mohamed Mahfouda, and Salah Benhadida. "Numerical study of the non-Newtonian blood flow in a stenosed artery using two rheological models." *Thermal Science* 20, no. 2 (2016): 449-460. https://doi.org/10.2298/TSCI130227161A

[21] Sankar, D. S. "Perturbation analysis for pulsatile flow of Carreau fluid through tapered stenotic arteries." *International Journal of Biomathematics* 9, no. 04 (2016): 1650063. https://doi.org/10.1142/S1793524516500637

[22] Neeraja, G., P. A. Dinesh, K. Vidya, and C. S. K. Raju. "Peripheral layer viscosity on the stenotic blood vessels for Herschel-Bulkley fluid model." *Informatics in Medicine Unlocked* 9 (2017): 161-165. https://doi.org/10.1016/j.imu.2017.08.004

[23] Veena, B. S., and Arundhati Warke. "The flow behaviour of blood in two-phase time-dependent tapered stenosed artery in the presence of transverse magnetic field." *Journal of Mathematical and Computational Science* 11, no. 1 (2020): 543-562.

[24] Singh, Ram, G. C. Sharma, and M. Jain. "Mathematical modeling of blood flow in a stenosed artery under MHD effect through porous medium." *International Journal of Engineering* 23, no. 3 (2010): 243-252.

[25] Chhabra, Raj P., and John Francis Richardson. *Non-Newtonian flow and applied rheology: engineering applications*. Butterworth-Heinemann, 2008.

[26] Misra, J. C., A. Sinha, and G. C. Shit. "Mathematical modeling of blood flow in a porous vessel having double stenoses in the presence of an external magnetic field." *International Journal of Biomathematics* 4, no. 02 (2011): 207-225. https://doi.org/10.1142/S1793524511001428

[27] Sankar, D. S., and K. Hemalatha. "Pulsatile flow of Herschel-Bulkley fluid through catheterized arteries-A mathematical model." *Applied Mathematical Modelling* 31, no. 8 (2007): 1497-1517. https://doi.org/10.1016/j.apm.2006.04.012